Rate of Immune Complex Cycling in Follicular Dendritic Cells Determines the Extent of Protecting Antigen Integrity and Availability to Germinal Center B Cells

Theinmozhi Arulraj,* Sebastian C. Binder,*,† and Michael Meyer-Hermann*,†,‡

Follicular dendritic cells (FDCs) retain immune complexes (ICs) for prolonged time periods and are important for germinal center (GC) reactions. ICs undergo periodic cycling in FDCs, a mechanism supporting an extended half-life of Ag. Based on experimental data, we estimated that the average residence time of PE-ICs on FDC surface and interior were 21 and 36 min, respectively. GC simulations show that Ag cycling might impact GC dynamics because of redistribution of Ag on the FDC surface and by protecting Ag from degradation. Ag protection and influence on GC dynamics varied with Ag cycling time and total Ag concentration. Simulations predict that blocking Ag cycling terminates the GC reaction and decreases plasma cell production. Considering that cycling of Ag could be a target for the modulation of GC reactions, our findings highlight the importance of understanding the mechanism and regulation of IC cycling in FDCs. ***The Journal of Immunology*****, 2021, 206: 1436–1442.**

Follicular dendritic cells (FDCs) form a dense network of cytoplasmic extensions in the B cell follicle (1–3) and are known for their ability to retain native Ag for a long period of time (1, 4, 5). FDCs were found to originate from perivascular mural cells in the spleen (6) and marginal reticular cells in the lymph node (7). Ag is distributed mainly in the form of immune complexes (ICs) nonuniformly on FDC processes (5). FDCs bind Ag by CR1/2 (8) and/or FcγRIIBs (9), depending on activation and availability of complement proteins (10). Although Ag is rapidly cleared from different body sites following immunization (11), long-term Ag-retention capacity of FDCs was believed to be due to a mechanism that protects Ag from damage (5). However, it was not understood how the ICs retained on FDC surface were maintained intact and stable for a long period (5).

Phan et al. (12) discovered that ICs captured by subcapsular sinus macrophages are transferred to follicular B cells, and in turn, FDCs acquire these ICs through complement receptors. Heesters et al. (13) found that ICs acquired by murine FDCs are rapidly internalized, and they reappear on the FDC surface. Experiments showed that ICs undergo multiple rounds of cycling in FDCs with significant amount of Ag remaining undegraded (13). Further, cycling of ICs was blocked by cytochalasin, an actin inhibitor, but the exact mechanism of IC cycling in FDCs is unknown (13). This finding suggested that cycling of ICs could be a process explaining the long-term Ag-retention ability of FDCs. Cycling in FDCs was also found to be involved in protecting infectious agents such as HIV virions, and FDCs could act as a constant source of HIV virions for infecting T follicular helper (Tfh) cells (14). Although the timescale of IC cycling is unknown, it has been shown with nanoparticle-tagged Ag that particle size could determine localization of Ag in FDCs (15). Larger size particles preferentially localized on FDC surface, and comparatively smaller particles are localized both in the interior and on the FDC surface (15).

FDCs are thought to be important for sustaining germinal center (GC) reactions and memory responses (16–19). GC B cells acquire Ag from FDCs in the form of ICs, and this is believed to drive affinity maturation of B cells in the GCs (20). Importance of Ag availability in enhancing GC reactions has been demonstrated by several studies (21–23). Several accessory activities of FDCs other than IC trapping, such as supply of BAFF (24–26) and maintaining follicular structure (27) and their importance, are being studied (17). In addition to primary and secondary lymphoid organs, FDCs are also found in tertiary lymphoid organs (28–30). Targeting FDCs in tertiary lymphoid organs is considered as a promising strategy to disrupt such ectopic GCs (31, 32).

Mathematical modeling remains instrumental in explaining several biological processes. Particularly, in silico studies on endocytosis and recycling of various receptor molecules have provided insights into the mechanism, implications, or timescale of the process and aided the interpretation of experimental data (33–37). In this study, we performed in silico experiments and estimated the cycling timescale of ICs in FDCs for the particular

*Department of Systems Immunology, Braunschweig Integrated Centre of Systems Biology, Helmholtz Centre for Infection Research, 38106 Braunschweig, Germany; †Centre for Individualized Infection Medicine, 30625 Hannover, Germany; and ‡Institute for Biochemistry, Biotechnology and Bioinformatics, Braunschweig University of Technology, 38106 Braunschweig, Germany

ORCIDs: 0000-0003-1169-1786 (S.C.B.); 0000-0002-4300-2474 (M.M.-H.).

Received for publication December 1, 2020. Accepted for publication January 22, 2021.

This work was supported by the European Union's Horizon 2020 Research and Innovation Programme under Marie Sklodowska-Curie Grant Agreement 765158 (to T.A.).

T.A., S.C.B., and M.M.-H. designed the study. T.A. performed simulations. S.C.B. and M.M.-H. supervised the project. T.A., S.C.B., and M.M.-H. wrote the manuscript.

Address correspondence and reprint requests to Prof. Michael Meyer-Hermann, Department of Systems Immunology, Braunschweig Integrated Centre of Systems Biology, Helmholtz Centre for Infection Research, Rebenring 56, 38106 Braunschweig, Lower Saxony, Germany. E-mail address: mmh@theoretical-biology.de

The online version of this article contains supplemental material.

Abbreviations used in this article: DZ, dark zone; FDC, follicular dendritic cell; G, green; GC, germinal center; IC, immune complex; LZ, light zone; MFI, mean fluorescence intensity; PC, plasma cell; Tfh, T follicular helper; Tfr, T follicular regulatory.

Ag PE. Using an agent-based model of GC reaction, we studied the implications of Ag cycling on GC reactions under different conditions.

Materials and Methods

Model for Ag cycling and estimation of cycling times

An agent-based approach was used to estimate cycling times in which individual Ag particles undergo transition between two states—interior and surface, corresponding to transition of Ag between the FDC interior and surface, respectively (Fig. 1A). Transition times t_{surface} and t_{interior} were sampled independently from gaussian distributions $N(\mu_s, \sigma_s)$ and $N(\mu_i, \sigma_i)$, respectively.

In silico experiments (described below) were performed following the experimental setup in (13) and parameters μ_s, σ_s, μ_i, and σ_i were varied to identify parameter sets with minimum cost with respect to the experimental results by an exhaustive parameter search. Parameters μ_s and μ_i were systematically varied between few minutes to 1 h, and σ_s and σ_i were varied between 0 and 80% of the corresponding mean (μ_s and μ_i, respectively). Cost of simulation results (S_k) with respect to experimental results (E_k) was calculated as follows:

$$cost = \sum_{k=1}^{n} \left(\frac{E_k - S_k}{E_k} \right)^2 \quad (1)$$

where n is the cumulative number of data points from all considered experiments. To set a cutoff for parameter estimates, parameter sets with ΔAkaike information criterion <2 with respect to the lowest cost parameter set were chosen for further consideration (Fig. 1D–G).

In silico experiments

Sequential staining simulation. The simulation corresponds to the sequential staining of PE-ICs on FDCs in (13). In the experiment, the authors incubated FDCs with three distinctly labeled Abs (with colors green [G], blue, and red) one at a time sequentially to stain surface ICs. Each staining was performed with a particular labeled Ab for 5 min, followed by a 60-min period in which no Ab is added. This resulted in ICs acquiring different combination of colors, depending on the localization of ICs during the time period of staining. Color combinations of PE particles were determined by visualizing the fluorescence of PE particles (13).

Addition of the labeled Abs was simulated in silico following the experimental setup (13), and Ag particles in state surface were assumed to acquire the corresponding color of the Ab. The binding probability of staining Abs was assumed to be 1, provided the Ag is in the state surface at any time during the 5-min staining periods. As the color combinations of 700 PE particles were examined in (13), 700 Ag particles were simulated and classified based on the color combination acquired as G–blue–red, none, G, G–blue, red, G–red, blue–red, and blue.

Acid wash simulation. The simulation follows the acid-stripping experiment performed in (13) to demonstrate the appearance of ICs on surface from interior of FDCs. The authors treated FDCs briefly with acid buffer, which removes the ICs from the FDC surface, and surface Ag was detected by quantifying mean fluorescence intensity (MFI) of PE staining after a 30-min recovery period (13).

In the simulations, acid wash was performed by removing the Ag particles in the state surface, and then the system was allowed to recover for 30 min before determining surface particle count. Surface particle count determined after acid wash, and recovery was normalized using the surface particle count determined in the absence of acid wash. Correspondingly, MFI data (13) of experiment were normalized with MFI from control (wild type), to compare with the normalized surface particle count from the simulations.

As the initial distribution of Ag particles on FDC surface and in the interior at the start of the experiment is unknown, in both the simulations described above, particles were distributed randomly in the states interior and surface using a probability sampled from uniform distribution. Simulations corresponding to each experiment were repeated 100 times.

GC simulations

We generated, to our knowledge, a new agent-based model of the GC reaction that uses elements from previous state-of-the-art models (38–40) and was particularly developed to cover the dynamics of Ag on FDCs. This model includes a three-dimensional discretized lattice, which is divided equally into a dark zone (DZ) and a light zone (LZ). For the affinity representation of B cells, a four-dimensional shape space (41) is used in which the position of the B cell with respect to a predefined optimal position provides a measure for the Ag binding probability. Initially, 250 Tfh cells are randomly incorporated in the lattice. Tfh migrate and tend to accumulate in the LZ because of chemotaxis.

In the LZ region, 200 FDCs are randomly distributed. Each FDC has six dendrites that are each 40 μm long. Each FDC occupies more than one lattice site; hence, there are several connected fragments distributed on several nodes for a single FDC. Rate constants of internalization and externalization for Ag are calculated from the average time spent on surface and interior of FDCs estimated from (13). For the simulations, average times of 36 and 21 min in the interior and surface were used, and each FDC is loaded with 3000 or 1000 Ag portions. The Ag portions are distributed equally in different fragments of every FDC. Surface Ag amount on each FDC (A_{surface}) was calculated by the following equation, where A_{Total} is the total Ag amount of an FDC and k_{ext} and k_{int} are the externalization and internalization rate constants, respectively.

$$\frac{dA_{\text{surface}}}{dt} = k_{\text{ext}}(A_{\text{Total}} - A_{\text{surface}}) - k_{\text{int}} A_{\text{surface}} \quad (2)$$

The calculated surface Ag amount is redistributed on all fragments of the FDC. In simulations without Ag cycling, we used the surface Ag amount $A_{\text{surface}} = A_{\text{Total}}$.

Degradation of Ag was modeled by a decrease in the surface Ag amount on FDCs over time as follows:

$$\frac{dA_{\text{surface}}}{dt} = -k_{\text{deg}} A_{\text{surface}} \quad (3)$$

where $k_{\text{deg}} = \frac{\ln 2}{t_{\text{deg}}}$, and t_{deg} is the Ag half-life.

Founder B cells with randomly chosen position and affinity are incorporated at a rate of two cells per hour for 96 h. Founder cells are assumed to divide six times before differentiating to LZ phenotype. During every cell division, B cells mutate with a probability 0.5 (42, 43), which would result in a shift in the shape space position.

LZ B cells collect Ag for a duration of 0.7 h by establishing contact with the FDCs, depending on the binding probability of the B cell. Acquisition of Ag by B cell reduces the amount of Ag at a particular fragment of FDC. Failure to collect Ag within the fixed duration leads to a switch to the apoptotic state, whereas successful Ag collection leads to the FDC-selected state. FDC-selected B cells establish contact with a neighboring Tfh cell and remain bound for 36 min. During this period, Tfh signals only the B cell with highest amount of Ag collected. At the end of interaction time with Tfh, if the B cell has received signals for <30 min, it becomes apoptotic. B cells that received sufficient signals are selected, retain the LZ phenotype for 6 h, and then recycle back to the DZ. Number of divisions of the recycled cell is determined by the amount of Ag collected, with the maximum number of divisions limited to six. After selection, mutation probability is reduced in an affinity-dependent manner. Seventy-two percent of the divisions are assumed to be asymmetric, after which one daughter cell retains all the Ag. Daughter cells retaining Ag differentiate to output/plasma cells (PCs) that exit the GC, whereas the other daughter cells acquire an LZ phenotype and proceed for the next round of selection. Steady-state distributions of chemokines CXCL12 and CXCL13 are calculated and used for the chemotaxis of motile cells. Detailed assumptions of GC B cell dynamics and parameter values follow the supplementary text of (44), with the newly introduced dynamics of Ag in FDCs described in this study.

Simulations were performed using C++. The ggplot2, plot3D, and Bolstad2 packages of R were used for analysis and visualization of the results.

Results

Estimation of cycling time of PE-ICs in murine FDC

Periodic cycling of Ag in FDCs was demonstrated by sequential staining of PE-ICs on cultured FDCs with three distinctly labeled Abs and quantification of the number of Ag particles tagged with different Abs (13). The authors showed that upon acid stripping of ICs on FDCs and subsequent recovery, ICs reappear on FDC surface (13). The timescale of Ag cycling in FDCs is unknown, as it is not directly measured in the experiments. However, as these experiments are informative in providing an estimate of the underlying timescale, we performed in silico simulations following the same ex vivo experimental protocol (see *Materials and Methods*). We used a model in which Ag particles undergo transition between two states, interior and surface (Fig. 1A, detailed description in *Materials and Methods*), and transition times (t_{surface} and t_{interior})

follow gaussian distributions. We fitted the mean (μ_s and μ_i) and width (σ_s and σ_i) of the gaussian distributions of transition times to estimate the average time IC clusters spend on the FDC surface and in the interior. We performed an exhaustive parameter search to identify the set of parameters with minimum combined cost to the experiments simulated. Parameter set with lowest cost indicated that particles spend an average time of 21 and 36 min on FDC surface and interior, respectively. The estimates were confirmed with a differential evolution parameter search over a larger range of parameters. Estimated parameter ranges are shown in Fig. 1D–G. The width of the distributions estimated (σ_s and σ_i) were broad (Fig. 1F, 1G). The experimental data could not be fitted with fixed cycling times ($\sigma_s = 0$ and $\sigma_i = 0$), suggesting that the variability in Ag presentation kinetics is critical to reproduce the data. To see whether the fit (Fig. 1B, 1C) could be improved further, we tested various possibilities such as varying the initial distribution of particles in the two states, binding probability of staining Abs, and considering a bimodal distribution for the average time in the state interior. All these trials resulted in similar or higher cost values and could not improve the fit to the data. However, the deviation from the experimental mean for the number of particles labeled blue (represented as B in Fig. 1B) could be due to large fluctuations in the behavior of Ag particles.

Ag redistribution on FDCs enhances GC reaction

To investigate if the cycling of Ag can influence the GC dynamics, we simulated the GC reaction (see *Materials and Methods*) in the presence and absence of Ag cycling (Fig. 2). The mean transition times obtained as described in previous section were used to calculate the externalization and internalization rate constants k_{ext} and k_{int} in Eq. 2. Because of cycling, Ag in FDC was distributed on the surface and the interior, with the distribution dependent on k_{ext} and k_{int}. In the absence of cycling, all the Ag portions were distributed on the FDC surface. As a result, surface Ag amount on FDC was lower in the GC simulation with cycling when compared with simulation without cycling (Fig. 2B). In the presence of Ag cycling, the GC volume at the peak of the reaction and thereafter (Fig. 2A) was increased despite having lower surface Ag concentration. There were no marked changes in the affinity of PCs produced (Fig. 2E). The changes in GC volume were reflected in the PC production, showing an increased PC production with Ag cycling (Fig. 2D). Importantly, the lower surface Ag concentration did not impair GC reactions, as Ag is subsequently replaced on the FDC surface at a timescale much shorter than the lifetime of GC reaction.

To check if the enhancement in GC volume at later stages is due to the redistribution of Ag from time to time, we redistributed surface Ag at every time step in the simulations without Ag cycling [simulations labeled No cycling (redist) in Fig. 2]. There were no differences in GC volume, apoptotic cells, or number or affinity of PCs with cycling and without cycling in the presence of redistribution (Fig. 2), suggesting that the enhancement in GC volume and PC production seen are due to the redistribution of Ag on FDC surface rather than a direct effect of Ag cycling. Hence, compared with the static representation of all Ag portions on FDC surface, redistribution of Ag on FDC surface, which can be brought about by Ag cycling, can enhance the GC reaction.

GC dynamics remains unaltered with varying cycling times

As there is a possibility that the cycling rates might vary dramatically depending on the particle size, we also varied the cycling times to check the impact on GC reactions. We chose the following average cycling times in the interior and surface of FDCs: 1) 10 and 50 min, particles spend longer on surface; 2) 36 and 21 min, estimated from PE-IC data, slightly longer in the interior than surface; and 3) 50 and 10 min, particles spend much longer time in the interior of FDC. With varying cycling times, surface Ag amount is altered (Supplemental Fig. 1A). However, the GC dynamics and output of GCs remained unaffected (Supplemental Fig. 1B–D). Similarly, when cycling parameters were varied in the estimated range, no major changes were seen in the kinetics of GC and output quantity or quality despite large changes in surface Ag amount (Supplemental Fig. 1E–H). Small differences were observed between the different cycling times in the simulations with

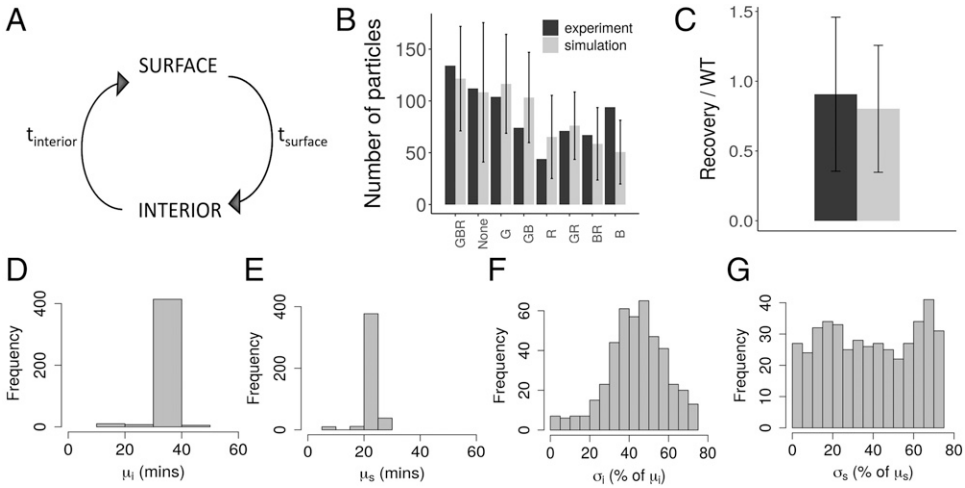

FIGURE 1. Estimation of PE-IC cycling time. (**A**) Schematic representation of the model used to estimate cycling times. (**B** and **C**) Simulation of sequential staining and acid wash (explained in *Materials and Methods*) compared with experimental data (13), for the parameter set with lowest cost (i.e., 21- and 36-min average time on surface and interior, respectively). (B) Sequential staining of ICs with Abs labeled G, blue (B), and red (R), and the readouts show the number of IC particles labeled with the corresponding color combinations indicated below the bars. (C) Acid-stripping of FDCs to remove ICs from surface, followed by a recovery period. Readout represents the surface particle count after acid stripping and recovery, normalized with the surface particle count of control without acid treatment. The measured MFI of the recovery sample was normalized with MFI of the wild type (WT) sample. (**D**–**G**) Parameter sets with ΔAkaike information criterion (AIC) <2 with respect to the lowest cost parameter set. (D) Average time in interior μ_i, (E) average time on FDC surface μ_s, (F) width of distribution for time in interior σ_i (as percentage of mean μ_i), and (G) width of distribution for time on FDC surface σ_s (as percentage of mean μ_s). $t_{interior}$, time spent by ICs in state interior; $t_{surface}$, time spent by ICs in state surface.

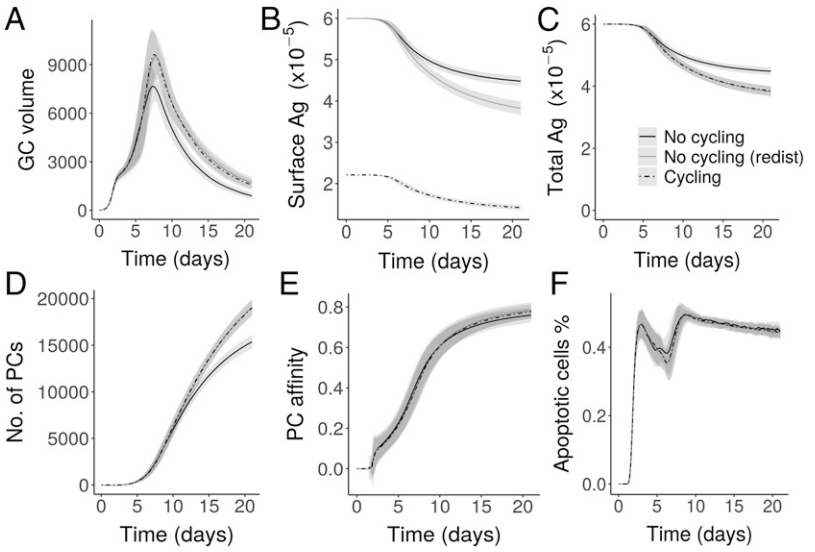

FIGURE 2. GC simulations in the presence and absence of Ag cycling: (**A**) GC volume measured by number of GC B cells, (**B**) surface Ag amount of all FDCs in the GC, (**C**) total Ag amount including surface Ag and internalized Ag, (**D**) number of PCs produced, (**E**) PC affinity, and (**F**) percentage of apoptotic cells. In the labels shown in (C), No cycling (redist) represents simulations without Ag cycling (similar to No cycling) but includes surface redistribution of Ag. Ag amount is represented as number of Ag portions.

lower Ag concentrations (data not shown). This shows that GC reactions are robust against changes in cycling times provided the Ag concentration is not limiting.

Cycling could impact GC reaction by limiting Ag degradation

Since the discovery of FDCs as long-term depots of Ag, it was not understood how easily degradable Ag is retained on FDC surface for a long period of time (5). It has been shown that constitutive endocytosis of vascular endothelial growth factor (VEGF) receptor protects the integrity of the receptor, and blocking this process results in the shedding of VEGF receptors (45). Similarly, the Ag could be protected by cycling, as this minimizes surface exposure. However, it is not clear how the Ag is protected from damage despite remaining available for GC reactions; hence, we tested if Ag cycling could protect Ag efficiently by minimizing Ag exposure on FDC surface without impairing GC reactions. Ag degradation was modeled using Eq. 3 (*Materials and Methods*) assuming that the surface Ag amount is degraded with a fixed half-life. The amount of degraded Ag was dependent on the cycling times (Fig. 3A), and the GC shutdown was delayed when the average time of Ag in the interior was higher (Fig. 3C). Consequently, there is an increase in PC production as well (Fig. 3D). Thus, in a system with Ag degradation, Ag cycling can increase the GC reaction duration and limit Ag degradation, extending the time period of Ag availability for B cell selection. Longer time for Ag inside the FDCs was advantageous for the GC output in this case (Fig. 3G–I). However, with low Ag concentration (Fig. 3J–L), a longer residence time inside FDCs would dramatically decrease the amount of Ag available for GC B cells, and hence, there is a trade-off between Ag protection and availability to GC B cells (Fig. 3).

Blocking Ag cycling can shut down GC reactions

We simulated the effect of blocking Ag cycling on GC reactions. When both internalization and externalization of Ag were blocked at different time points of the GC reaction, shutdown of GC reaction was accelerated (Fig. 4A), and PC production was decreased (Fig. 4C). Blockade of Ag cycling slightly impaired affinity maturation (Fig. 4D). The impact on the GC reaction varied depending on the time point of blockade. Blocking internalization of Ag alone did not have any impact on the GC reactions (data not shown). Blocking Ag externalization alone results in the accumulation of Ag in the interior of FDCs and results in a quick termination of GC reactions (Supplemental Fig. 2) when compared with blocking both internalization and externalization. These results suggest that Ag cycling can also be blocked to terminate GC reactions in a way similar to the effect of Ab feedback (46–48).

Discussion

Discovery of IC cycling in FDCs (13) has shed light on the previously unexplained observation of extended half-life of FDC Ag. In this study, we demonstrate the importance of IC cycling in GC reactions by performing in silico simulations. Our findings suggest that understanding the cycling of ICs in FDCs could have numerous implications in modulating GC reactions for efficient response toward vaccination and dissolving chronic GCs and for devising strategies to target pathogens such as HIV that remain protected in the FDCs (14).

Analysis of published experimental results (13) revealed the time scale of IC cycling in FDCs, which was previously unknown, and predicted that PE-IC particles spend ∼21 min on the FDC surface and 36 min in the interior of FDCs. In the predicted range of Ag-display kinetics, GC simulations showed robust dynamics and output production, suggesting that cycling might not impact the GC dynamics directly in the presence of high total Ag concentration. Consistently, changes in IC deposition in experiments did not lead to large alterations in the GC responses (49).

Considering that Ag integrity might be affected by prolonged exposure on FDC surface, our simulations demonstrate how Ag cycling could protect Ag degradation by minimizing surface exposure and at the same time allowing for efficient Ag uptake by GC B cells. Experimental data on time course of the number of GCs suggest that GCs are formed for at least until day 12 after immunization (50). Particularly, such late initialized GCs might be highly impaired if Ag is not retained stable for a long period.

According to our results, protection of Ag from degradation was largely dependent on the cycling rates, and degradation is minimum if the Ag tends to spend longer time in the interior of FDCs. With limiting total Ag concentration, cycling rates determined the trade-off between protecting Ag from damage and allowing the efficient uptake of Ag by GC B cells. It is currently unknown whether ICs other than PE-ICs have a different cycling kinetics. However, Ag tagged to nanoparticles of different sizes differ in the distribution of these particles between the FDC surface and interior (15). In addition to the cycling rates, variation in Ag degradation rates suggested that surface Ag half-life might also impact the GC dynamics. As different Ags might have different half-lives at FDC

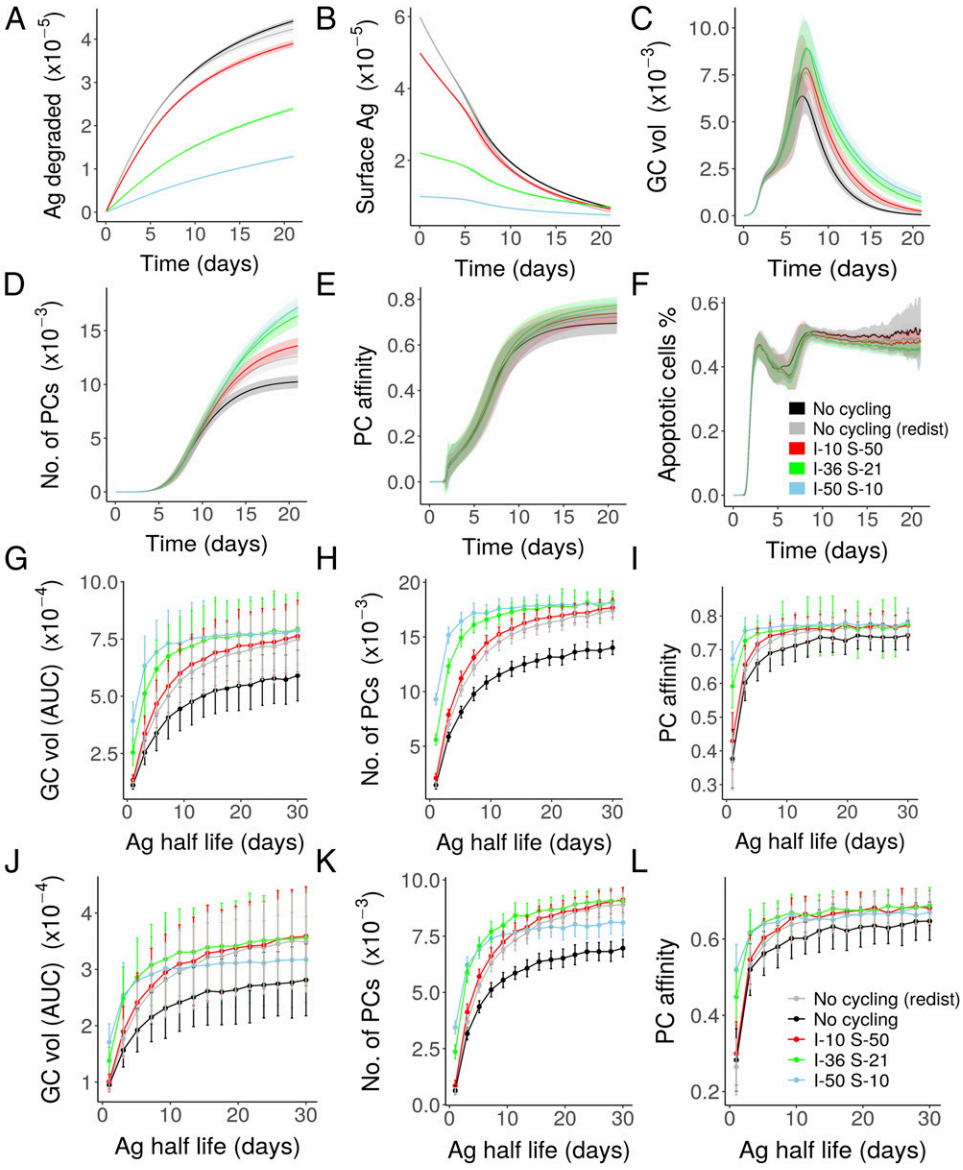

FIGURE 3. GC simulations in the presence of Ag degradation (Eq. 3) with a half-life of 8 d: (**A**) amount of Ag degraded, (**B**) surface Ag amount, (**C**) GC volume, (**D**) number of PCs produced, (**E**) affinity of PCs, and (**F**) percentage of apoptotic cells. (**G–L**) Dependence of GC volume kinetics and output on cycling rates and Ag half-life for different Ag concentrations: area under curve (AUC) of the GC volume kinetics (G and J), number of PCs (H and K), and PC affinity (I and L) observed on day 21 of the GC reaction. Legend shows average time spent by Ag particles in the interior (I) and surface (S) of FDCs (in minutes). Total Ag portion is 3000 and 1000 in each FDC for (A)–(I) and (J)–(L), respectively.

surface and cycling rates, interplay between these factors might determine the stability of different Ags on FDCs. Dynamics of transport of Ag to the lymphoid follicles (51–53) and retention and presentation on FDCs vary with the nature and size of Ag particles (15), and these observations could be employed to engineer nanoparticles promoting efficient Ag retention in the FDCs in the context of vaccination (15). As our study relies on a limited set of experimental data on PE-ICs, further studies examining cycling kinetics with different Ags and experimental settings would greatly facilitate engineering Ags to enhance GC responses and improve the success of vaccination. Characterizing the cycling kinetics of clinically relevant Ags such as HIV, prions, and autoantigens could also be useful for designing therapeutic interventions against these pathogenic agents.

Moreover, blocking IC cycling prevents the efficient uptake and acquisition of Ag by FDCs (13). Hence, the importance of Ag cycling in FDCs on GC reactions could be more than what is estimated by our simulations. Further studies are needed to address the role of Ag cycling in initial acquisition of Ag by FDCs and its contribution to the efficiency of GC and memory responses. In the light of several studies showing that Ag delivery can be modulated to alter GC responses (21, 22), our findings contribute to understanding the dynamics of Ag within the FDCs brought about by cycling and its impact on the GC reaction kinetics. In addition to the GC reactions, long-term protection of Ag due to Ag cycling might be of importance in maintaining the memory responses. It has been shown that memory B cells reside close to contracted GCs (54), and it is thought that they might be reactivated upon exposure to Ag to maintain the serum Ab concentration levels (17, 55).

In the simulations, Ag cycling blockade at different time points resulted in termination of GC reactions. However, as the precise mechanism of Ag cycling is currently unknown, understanding the mechanism and gaining more insights into the factors regulating Ag cycling could help identify targets that might provide a therapeutic opportunity to dissolve Ag-dependent chronic GCs. Presently, it is

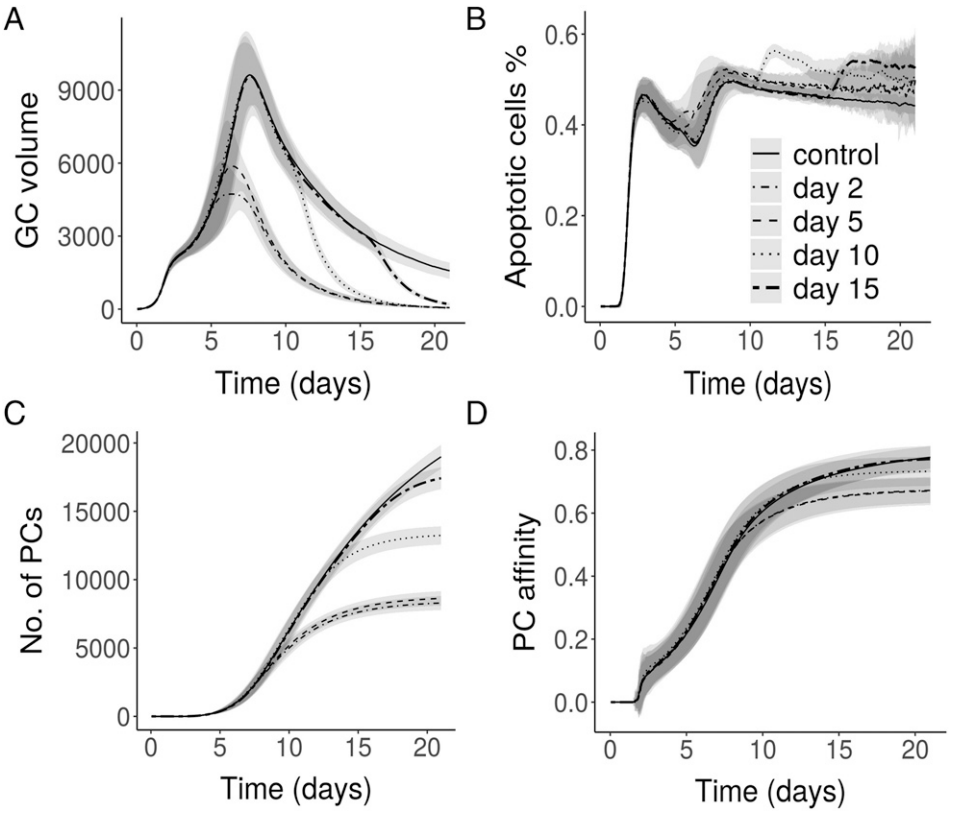

FIGURE 4. Effect of blocking both Ag internalization and externalization: (**A**) GC volume, (**B**) percentage of apoptotic cells, (**C**) number of PCs, and (**D**) affinity of PCs. Legend represents the time of blockade.

unknown whether the cycling IC is bound to complement receptor or FcγR and whether the fate of internalized Ag in FDCs varies depending on the receptor. In the case of dendritic cells, both nondegradative and degradative pathways exist for internalized Ag that are mediated by inhibitory FcγRIIB and activating FcγRs, respectively (56). Future studies tracking the distribution of these receptors on FDCs and colocalization with Ag could be an immediate follow-up in view of delineating the IC-cycling mechanism. Further, the mechanism and extent of Ag retention in the absence of FcγR and complement receptors on FDCs also needs to be investigated.

We have assumed that IC distribution is similar among different regions of the FDC. Considering the impact of IC redistribution in influencing GC reactions as predicted by our simulations, examining the distribution of ICs among different regions of FDC and among the FDCs in DZ and LZ would be helpful in further characterizing the IC distribution and implications of IC cycling. The reason behind the nonuniform distribution of ICs on FDCs despite the redistribution because of IC cycling also needs to be investigated.

The rate of IC cycling was assumed to be constant in the simulations throughout the course of the GC reaction. It remains to be explored whether the maturation state of FDCs influences the IC-cycling rate such that IC presentation dynamics varies at different phases of the GC reaction. Consequently, because of changes in IC-cycling rates, fate of GC B cells might be expected to vary at different stages of the GC reaction. As the maturation state of FDCs varies because of the influence of cytokines and interactions with B cells, future studies on the dependence of FDC development on various factors and how this influences IC-cycling rates might shed light on the regulation of IC cycling by other cell types. In this context, it might be interesting to test the changes in FDC development and Ag cycling dynamics when the GC maintenance is disrupted, as in the case of absence of T cells or other defects. Muñoz-Fernández et al. (57) showed that contractility of FDCs is enhanced by IL-2 and decreased by IL-10, suggesting cytokine-dependent changes in FDC morphology. IL-10 produced by T follicular regulatory (Tfr) cells (58) and a subset of human tonsillar follicular T cells (59) might be able to influence Ag-display dynamics on FDCs in the GCs. Several mechanisms of action of Tfr cells in regulating GCs have been proposed, including the direct inhibition of GC B cells and Tfh cells (60–62). In addition to these mechanisms, a potential impact of Tfr cells on FDCs and Ag display might also play a role. Moreover, a dynamic regulation of Ag cycling in the GCs during the course of the GC reaction could be expected, depending on cytokine levels.

A number of factors, including Ab feedback (46–48) and CD40/CD40L interactions (63, 64), are able to influence GC shutdown even though the mechanism of shutdown is not well understood. As Ag was detectable in FDCs of lymphoid follicles even after the GC reaction ends (4), it is believed that the termination of GCs is not primarily due to the lack of Ag. However, future studies might explore whether natural alterations of Ag presentation by cytokines and other factors could promote the termination of GC reactions.

Acknowledgments

We thank Michael Carroll and Balthasar Heesters for discussions and clarifying the experimental protocol. We also thank Sahamoddin Khailaie for constructive suggestions.

Disclosures

The authors have no financial conflicts of interest.

References

1. Kosco, M. H., and D. Gray. 1992. Signals involved in germinal center reactions. *Immunol. Rev.* 126: 63–76.
2. Cyster, J. G., K. M. Ansel, K. Reif, E. H. Ekland, P. L. Hyman, H. L. Tang, S. A. Luther, and V. N. Ngo. 2000. Follicular stromal cells and lymphocyte homing to follicles. *Immunol. Rev.* 176: 181–193.

3. Chen, L. L., J. C. Adams, and R. M. Steinman. 1978. Anatomy of germinal centers in mouse spleen, with special reference to "follicular dendritic cells". *J. Cell Biol.* 77: 148–164.
4. Tew, J. G., and T. E. Mandel. 1979. Prolonged antigen half-life in the lymphoid follicles of specifically immunized mice. *Immunology* 37: 69–76.
5. Mandel, T. E., R. P. Phipps, A. P. Abbot, and J. G. Tew. 1981. Long-term antigen retention by dendritic cells in the popliteal lymph node of immunized mice. *Immunology* 43: 353–362.
6. Krautler, N. J., V. Kana, J. Kranich, Y. Tian, D. Perera, D. Lemm, P. Schwarz, A. Armulik, J. L. Browning, M. Tallquist, et al. 2012. Follicular dendritic cells emerge from ubiquitous perivascular precursors. *Cell* 150: 194–206.
7. Jarjour, M., A. Jorquera, I. Mondor, S. Wienert, P. Narang, M. C. Coles, F. Klauschen, and M. Bajénoff. 2014. Fate mapping reveals origin and dynamics of lymph node follicular dendritic cells. *J. Exp. Med.* 211: 1109–1122.
8. Fang, Y., C. Xu, Y.-X. Fu, V. M. Holers, and H. Molina. 1998. Expression of complement receptors 1 and 2 on follicular dendritic cells is necessary for the generation of a strong antigen-specific IgG response. *J. Immunol.* 160: 5273–5279.
9. Qin, D., J. Wu, K. A. Vora, J. V. Ravetch, A. K. Szakal, T. Manser, and J. G. Tew. 2000. Fc γ receptor IIB on follicular dendritic cells regulates the B cell recall response. *J. Immunol.* 164: 6268–6275.
10. Yoshida, K., T. K. van den Berg, and C. D. Dijkstra. 1993. Two functionally different follicular dendritic cells in secondary lymphoid follicles of mouse spleen, as revealed by CR1/2 and FcR gamma II-mediated immune-complex trapping. *Immunology* 80: 34–39.
11. Tew, J. G., T. E. Mandel, and P. L. Rice. 1980. Immune elimination and immune retention: the relationship between antigen retained in the foot and the elicitation of footpad swelling. *Immunology* 40: 425–433.
12. Phan, T. G., I. Grigorova, T. Okada, and J. G. Cyster. 2007. Subcapsular encounter and complement-dependent transport of immune complexes by lymph node B cells. *Nat. Immunol.* 8: 992–1000.
13. Heesters, B. A., P. Chatterjee, Y.-A. Kim, S. F. Gonzalez, M. P. Kuligowski, T. Kirchhausen, and M. C. Carroll. 2013. Endocytosis and recycling of immune complexes by follicular dendritic cells enhances B cell antigen binding and activation. *Immunity* 38: 1164–1175.
14. Heesters, B. A., M. Lindqvist, P. A. Vagefi, E. P. Scully, F. A. Schildberg, M. Altfeld, B. D. Walker, D. E. Kaufmann, and M. C. Carroll. 2015. Follicular dendritic cells retain infectious HIV in cycling endosomes. *PLoS Pathog.* 11: e1005285.
15. Zhang, Y.-N., J. Lazarovits, W. Poon, B. Ouyang, L. N. M. Nguyen, B. R. Kingston, and W. C. W. Chan. 2019. Nanoparticle size influences antigen retention and presentation in lymph node follicles for humoral immunity. *Nano Lett.* 19: 7226–7235.
16. Kosco-Vilbois, M. H., H. Zentgraf, J. Gerdes, and J.-Y. Bonnefoy. 1997. To 'B' or not to 'B' a germinal center? *Immunol. Today* 18: 225–230.
17. Kosco-Vilbois, M. H. 2003. Are follicular dendritic cells really good for nothing? *Nat. Rev. Immunol.* 3: 764–769.
18. Gray, D., M. Kosco, and B. Stockinger. 1991. Novel pathways of antigen presentation for the maintenance of memory. *Int. Immunol.* 3: 141–148.
19. Gray, D. 2002. A role for antigen in the maintenance of immunological memory. *Nat. Rev. Immunol.* 2: 60–65.
20. MacLennan, I. C. M. 1994. Germinal centers. *Annu. Rev. Immunol.* 12: 117–139.
21. Cirelli, K. M., D. G. Carnathan, B. Nogal, J. T. Martin, O. L. Rodriguez, A. A. Upadhyay, C. A. Enemuo, E. H. Gebru, Y. Choe, F. Viviano, et al. 2019. Slow delivery immunization enhances HIV neutralizing antibody and germinal center responses via modulation of immunodominance. [Published erratum appears in 2020 *Cell* 180: 206.] *Cell* 177: 1153–1171.e28.
22. Tam, H. H., M. B. Melo, M. Kang, J. M. Pelet, V. M. Ruda, M. H. Foley, J. K. Hu, S. Kumari, J. Crampton, A. D. Baldeon, et al. 2016. Sustained antigen availability during germinal center initiation enhances antibody responses to vaccination. *Proc. Natl. Acad. Sci. USA* 113: E6639–E6648.
23. Cirelli, K. M., and S. Crotty. 2017. Germinal center enhancement by extended antigen availability. *Curr. Opin. Immunol.* 47: 64–69.
24. Hase, H., Y. Kanno, M. Kojima, K. Hasegawa, D. Sakurai, H. Kojima, N. Tsuchiya, K. Tokunaga, N. Masawa, M. Azuma, et al. 2004. BAFF/BLyS can potentiate B-cell selection with the B-cell coreceptor complex. *Blood* 103: 2257–2265.
25. Gorelik, L., K. Gilbride, M. Dobles, S. L. Kalled, D. Zandman, and M. L. Scott. 2003. Normal B cell homeostasis requires B cell activation factor production by radiation-resistant cells. *J. Exp. Med.* 198: 937–945.
26. Lesley, R., Y. Xu, S. L. Kalled, D. M. Hess, S. R. Schwab, H.-B. Shu, and J. G. Cyster. 2004. Reduced competitiveness of autoantigen-engaged B cells due to increased dependence on BAFF. *Immunity* 20: 441–453.
27. Wang, X., B. Cho, K. Suzuki, Y. Xu, J. A. Green, J. An, and J. G. Cyster. 2011. Follicular dendritic cells help establish follicle identity and promote B cell retention in germinal centers. *J. Exp. Med.* 208: 2497–2510.
28. Aziz, K. E., P. J. McCluskey, and D. Wakefield. 1997. Characterisation of follicular dendritic cells in labial salivary glands of patients with primary Sjögren syndrome: comparison with tonsillar lymphoid follicles. *Ann. Rheum. Dis.* 56: 140–143.
29. Randen, I., O. J. Mellbye, O. Førre, and J. B. Natvig. 1995. The identification of germinal centres and follicular dendritic cell networks in rheumatoid synovial tissue. *Scand. J. Immunol.* 41: 481–486.
30. Pipi, E., S. Nayar, D. H. Gardner, S. Colafrancesco, C. Smith, and F. Barone. 2018. Tertiary lymphoid structures: autoimmunity goes local. *Front. Immunol.* 9: 1952.
31. Hughes, C. E., R. A. Benson, M. Bedaj, and P. Maffia. 2016. Antigen-presenting cells and antigen presentation in tertiary lymphoid organs. *Front. Immunol.* 7: 481.
32. Kranich, J., and N. J. Krautler. 2016. How follicular dendritic cells shape the B-cell antigenome. *Front. Immunol.* 7: 225.
33. Fehling-Kaschek, M., D. B. Peckys, D. Kaschek, J. Timmer, and N. Jonge. 2019. Mathematical modeling of drug-induced receptor internalization in the HER2-positive SKBR3 breast cancer cell-line. *Sci. Rep.* 9: 12709.
34. Schmidt-Glenewinkel, H., I. Vacheva, D. Hoeller, I. Dikic, and R. Eils. 2008. An ultrasensitive sorting mechanism for EGF receptor endocytosis. *BMC Syst. Biol.* 2: 32.
35. Beyer, T., and M. Meyer-Hermann. 2008. Cell transmembrane receptors determine tissue pattern stability. *Phys. Rev. Lett.* 101: 148102.
36. Khailaie, S., B. Rowshanravan, P. A. Robert, E. Waters, N. Halliday, J. D. Badillo Herrera, L. S. K. Walker, D. M. Sansom, and M. Meyer-Hermann. 2018. Characterization of CTLA4 trafficking and implications for its function. *Biophys. J.* 115: 1330–1343.
37. Lunov, O., V. Zablotskii, T. Syrovets, C. Röcker, K. Tron, G. U. Nienhaus, and T. Simmet. 2011. Modeling receptor-mediated endocytosis of polymer-functionalized iron oxide nanoparticles by human macrophages. *Biomaterials* 32: 547–555.
38. Meyer-Hermann, M., E. Mohr, N. Pelletier, Y. Zhang, G. D. Victora, and K.-M. Toellner. 2012. A theory of germinal center B cell selection, division, and exit. *Cell Rep.* 2: 162–174.
39. Meyer-Hermann, M. 2014. Overcoming the dichotomy of quantity and quality in antibody responses. *J. Immunol.* 193: 5414–5419.
40. Binder, S. C., and M. Meyer-Hermann. 2016. Implications of intravital imaging of murine germinal centers on the control of B cell selection and division. *Front. Immunol.* 7: 593.
41. Perelson, A. S., and G. F. Oster. 1979. Theoretical studies of clonal selection: minimal antibody repertoire size and reliability of self-non-self discrimination. *J. Theor. Biol.* 81: 645–670.
42. Nossal, G. J. V. 1992. The molecular and cellular basis of affinity maturation in the antibody response. *Cell* 68: 1–2.
43. Berek, C., and C. Milstein. 1987. Mutation drift and repertoire shift in the maturation of the immune response. *Immunol. Rev.* 96: 23–41.
44. Meyer-Hermann, M., S. C. Binder, L. Mesin, and G. D. Victora. 2018. Computer simulation of multi-color brainbow staining and clonal evolution of B cells in germinal centers. *Front. Immunol.* 9: 2020.
45. Basagiannis, D., and S. Christoforidis. 2016. Constitutive endocytosis of VEGFR2 protects the receptor against shedding. *J. Biol. Chem.* 291: 16892–16903.
46. Zhang, Y., M. Meyer-Hermann, L. A. George, M. T. Figge, M. Khan, M. Goodall, S. P. Young, A. Reynolds, F. Falciani, A. Waisman, et al. 2013. Germinal center B cells govern their own fate via antibody feedback. *J. Exp. Med.* 210: 457–464.
47. Meyer-Hermann, M. 2019. Injection of antibodies against immunodominant epitopes tunes germinal centers to generate broadly neutralizing antibodies. *Cell Rep.* 29: 1066–1073.e5.
48. Arulraj, T., S. C. Binder, P. A. Robert, and M. Meyer-Hermann. 2019. Synchronous germinal center onset impacts the efficiency of antibody responses. *Front. Immunol.* 10: 2116.
49. Vora, K. A., J. V. Ravetch, and T. Manser. 1997. Amplified follicular immune complex deposition in mice lacking the Fc receptor gamma-chain does not alter maturation of the B cell response. *J. Immunol.* 159: 2116–2124.
50. Rao, S. P., K. A. Vora, and T. Manser. 2002. Differential expression of the inhibitory IgG Fc receptor FcgammaRIIB on germinal center cells: implications for selection of high-affinity B cells. *J. Immunol.* 169: 1859–1868.
51. Gonzalez, S. F., S. E. Degn, L. A. Pitcher, M. Woodruff, B. A. Heesters, and M. C. Carroll. 2011. Trafficking of B cell antigen in lymph nodes. *Annu. Rev. Immunol.* 29: 215–233.
52. Gonzalez, S. F., V. Lukacs-Kornek, M. P. Kuligowski, L. A. Pitcher, S. E. Degn, S. J. Turley, and M. C. Carroll. 2010. Complement-dependent transport of antigen into B cell follicles. *J. Immunol.* 185: 2659–2664.
53. Link, A., F. Zabel, Y. Schnetzler, A. Titz, F. Brombacher, and M. F. Bachmann. 2012. Innate immunity mediates follicular transport of particulate but not soluble protein antigen. J. Immunol. 188: 3724–3733.
54. Aiba, Y., K. Kometani, M. Hamadate, S. Moriyama, A. Sakaue-Sawano, M. Tomura, H. Luche, H. J. Fehling, R. Casellas, O. Kanagawa, A. Miyawaki, and T. Kurosaki. 2010. Preferential localization of IgG memory B cells adjacent to contracted germinal centers. *Proc. Natl. Acad. Sci. USA* 107: 12192–12197.
55. Szakal, A. K., and J. G. Tew. 1992. Follicular dendritic cells: B-cell proliferation and maturation. *Cancer Res.* 52(Suppl.): 5554s–5556s.
56. Bergtold, A., D. D. Desai, A. Gavhane, and R. Clynes. 2005. Cell surface recycling of internalized antigen permits dendritic cell priming of B cells. *Immunity* 23: 503–514.
57. Muñoz-Fernández, R., A. Prados, I. Tirado-González, F. Martín, A. C. Abadía, and E. G. Olivares. 2014. Contractile activity of human follicular dendritic cells. *Immunol. Cell Biol.* 92: 851–859.
58. Laidlaw, B. J., Y. Lu, R. A. Amezquita, J. S. Weinstein, J. A. Vander Heiden, N. T. Gupta, S. H. Kleinstein, S. M. Kaech, and J. Craft. 2017. Interleukin-10 from $CD4^+$ follicular regulatory T cells promotes the germinal center response. *Sci. Immunol.* 2: eaan4767.
59. Cañete, P. F., R. A. Sweet, P. Gonzalez-Figueroa, I. Papa, N. Ohkura, H. Bolton, J. A. Roco, M. Cuenca, K. J. Bassett, I. Sayin, et al. 2019. Regulatory roles of IL-10-producing human follicular T cells. *J. Exp. Med.* 216: 1843–1856.
60. Sage, P. T., A. M. Paterson, S. B. Lovitch, and A. H. Sharpe. 2014. The coinhibitory receptor CTLA-4 controls B cell responses by modulating T follicular helper, T follicular regulatory, and T regulatory cells. *Immunity* 41: 1026–1039.
61. Ritvo, P.-G. G., G. Churlaud, V. Quiniou, L. Florez, F. Brimaud, G. Fourcade, E. Mariotti-Ferrandiz, and D. Klatzmann. 2017. T_{fr} cells lack IL-2Rα but express decoy IL-1R2 and IL-1Ra and suppress the IL-1-dependent activation of T_{fh} cells. *Sci. Immunol.* 2: eaan0368.
62. Wing, J. B., M. Tekgüç, and S. Sakaguchi. 2018. Control of germinal center responses by T-follicular regulatory cells. *Front. Immunol.* 9: 1910.
63. Takahashi, Y., P. R. Dutta, D. M. Cerasoli, and G. Kelsoe. 1998. In situ studies of the primary immune response to (4-hydroxy-3-nitrophenyl)acetyl. V. Affinity maturation develops in two stages of clonal selection. *J. Exp. Med.* 187: 885–895.
64. Bolduc, A., E. Long, D. Stapler, M. Cascalho, T. Tsubata, P. A. Koni, and M. Shimoda. 2010. Constitutive CD40L expression on B cells prematurely terminates germinal center response and leads to augmented plasma cell production in T cell areas. *J. Immunol.* 185: 220–230.